Journal of
Applied Remote Sensing

Coastal wave field extraction using TerraSAR-X data

Miguel Bruck
Susanne Lehner

SPIE

Coastal wave field extraction using TerraSAR-X data

Miguel Bruck and Susanne Lehner
Remote Sensing Technology Institute, German Aerospace Center, Münchner Straße 20, Oberpfaffenhofen, Weßling 82234, Germany
miguel.bruck@dlr.de

Abstract. The main highlights of TerraSAR-X (TS-X) synthetic aperture radar (SAR) imagery are a higher resolution of up to 1 m, when compared to conventional C-band SAR data, and a reduction of nonlinear imaging effects of a moving target by lower platform altitude. Thus, ocean waves with wavelength <30 m are detectable. This makes TS-X particularly useful to observe coastal areas where complex bathymetry strongly impacts the approaching waves. TS-X images acquired in different coastal areas are presented, including three case studies at the German coast. Wave fields (significant wave height and peak wavelength) are derived from the TS-X imagery using the proposed XWAVE algorithm and compared not only to *in situ* buoy wave measurements but also to results of a high-resolution numerical wave model. The objective is to study the quality of significant wave height field estimation in the spatial domain in highly variable conditions, which are typically dominant in coastal areas. The results show that the empirical XWAVE algorithm allows estimating wave fields from TS-X data with high resolution, thus showing the spatial information on wave variations. Therefore, it is a new useful tool to characterize sea state in coastal areas by remote sensing. [DOI: 10.1117/1.JRS.7.073694]

Keywords: TerraSAR-X; synthetic aperture radar; significant wave height; sea state; coastal ocean areas.

Paper 13122P received Apr. 23, 2013; revised manuscript received Jul. 18, 2013; accepted for publication Jul. 19, 2013; published online Sep. 25, 2013.

1 Introduction

In the open ocean, in deep waters, and during nonstorm conditions, wave properties do not change significantly (e.g., significant wave height and wave period remain the same) in the order of several kilometers. In coastal areas, however, the wave properties change considerably, influenced by the underlying bathymetry. Waves in coastal waters normally experience effects such as shoaling, refraction, and diffraction. Additionally, ocean waves are often affected by currents and by crossing over other wave systems, nonlinear wave–wave interaction, and also depth-induced wave breaking.

It is a fact that it is not possible to measure with a buoy (ocean wave's measurement device) the variation of the sea state in the spatial domain. The buoy only provides information regarding sea state at its exact location. To measure variability of the sea state in high variable areas like coastal areas, an array of ocean waves measuring buoys can be used, although this method has limitations. More preferably, coastal wave numerical models are used.

In order for numerical wave models to predict accurately the wave field (e.g., significant wave height or peak wavelength) in coastal ocean areas, it needs not only correct input of wave and wind information for the model mesh boundary, but also an up-to-date fine meshed bathymetry (underwater topography).

In complex coastal areas, the bathymetry needs to have resolution in the order of a few hundred meters or less. Achieving this goal is not straightforward.

Normally bathymetry is obtained by field campaigns using methods (e.g., ships, probes, etc.) that are costly. In addition, the underwater terrain of some coastal areas is not really solid, and the topography changes in time through erosion and sediment (e.g., mud, sand). Another method to

obtain information regarding the sea state or wave field is by analyzing synthetic aperture radar (SAR) data. SAR data have been known since the first SAR missions to be able to provide ocean wave information to some extent.[1,2] Different algorithms were developed to derive sea-state information (e.g., significant wave height: H_s) from SAR data.[2–9] The algorithms were mostly developed and used to provide information about ocean waves on a global scale from SAR data acquired over open ocean.

The TerraSAR-X (TS-X) satellite provides high-resolution (up to 1 m) SAR images of the ocean surface, spatial resolution which was not available with the previous conventional C-band satellites, e.g., ERS and ENVISAT missions. This makes TS-X data especially suitable for coastal surface wave field observation, especially to observe the considerably changing sea-state properties.

Recently, some first studies using TS-X data for coastal applications were done focusing on wind, waves, wave refraction, and underwater topography estimation.[10–13]

However, these studies did not focus on significant wave height or the rapid change of sea-state properties in a higher-resolution scale (<2.5 km), which is the purpose of this paper.

An algorithm to derive significant wave height from TS-X data (XWAVE) is developed.[14] The algorithm is tuned and validated using *in situ* buoy wave measurements in deep water collocated with TS-X data. Validation with *in situ* wave measurement resulted in a good performance, with a correlation R of 93% and a scatter index of 0.22.

The algorithm achieved performance was accomplished when using TS-X data acquired under specific sea state conditions and limited data-set. Focusing on the conditions of the acquired TS-X data, those were the following: the data needs to be free of any nonwind generated ocean waves phenomena's artifacts, as internal waves, atmospherics disturbances, oil slicks, ships, off shore structures, etc. The limits for the significant wave heights analyzed in the data for the tuning/validation are between 1 m and 7.2 m, the limits of the sea surface wind speeds conditions are above 3.5 m/s and below 16 m/s. Additionally the sea type analyzed are mixed conditions of swell and wind sea which are typical for open ocean sea waters. Conditions outside these limits could be outside the expected performance that is why the algorithm tested in coastal areas, is a good challenge to assert the stability of the algorithm.

The new algorithm is an updated version of the algorithm in Ref. 15 with several differences, with the inclusion of the wind information (sea surface wind speed at 10 m height) of the analyzed subscene being one of the most important variations, It is obtained by using the XMOD algorithm.[16]

In this paper, we show an application using TS-X imagery to derive meteo-marine information from coastal areas, exploiting the advantage of the high-resolution TS-X SAR, allowing measurement of the variability of significant wave height and wavelength present in coastal areas. We show three case studies of TS-X imagery acquired over coastal areas and derive the significant wave height fields. The results are compared to *in situ* measurements or global/coastal model results. Additionally, we produce the corresponding peak wavelength fields for each subscene analyzed.

2 Data

The TS-X multilook ground range detected (MGD) Stripmap SAR product is used in our study. It covers usually an area of about 30×50 km and has an average pixel spacing of 1.25 m, an azimuth resolution of 3 m, and a range resolution between 1.7 and 3.5 m depending on the incidence angle of the acquisition. The radiometric accuracy is of about 0.6 dB.[17] More information regarding this data can be found in Ref. 18.

Wave numerical model data provided by the German Weather Center (DWD) are used in this paper, which are used to verify the results together with the *in situ* data. The wave numerical model used is a third-generation wave model, WAM.[19]

The data provided by the DWD were significant wave height, swell height, and wind sea height and respective peak directions, and additional wind information. The data have a spatial resolution of 0.75 deg and the model time output is every 3 h.

Data from the wave spectral model k-model are also used. The k-model is a third-generation wave prediction model, based on the action balance equation, designed especially for coastal

areas developed at the Helmholtz-Zentrum Geesthacht. More information and applications of this model can be found in Ref. 20. For our case studies, the wave model was set to run using an input with a grid size the same as the input bathymetry which is 1 nautical mile spatial resolution.

In situ buoy wave measurements are provided by the North West European Shelf Operational Oceanographic System through the site http://www.noos.cc/.

3 Algorithm to Derive Sea-State Information from TS-X Data: XWAVE

In this paper we apply the XWAVE algorithm, which was introduced in Ref. 14, to derive sea-state information from TS-X data.

The XWAVE algorithm is a two-step function, Eqs. (1) and (2), with a simple buffer region between the two functions Eq. (3) where Eqs. 1, 2, 3 are used according to the range of wave heights of the ocean area where the TS-X data are acquired. A more detailed explanation follows:

To know previously which is the range of the significant wave heights of the ocean area where TS-X data are acquired in order to know which formula to use, a parameter derived from the analysis of the TS-X data is used for this purpose, the azimuth cut-off wavelength.

The method used to derive the azimuth cut-off wavelength is, in simple terms, based on the spectral analysis of the two-dimensional (2-D) spectrum, where the width of the range band observed on the 2-D spectrum is proportional within a certain degree to significant wave height and sea surface wind speed. The azimuth cut-off wavelength was found in previous studies to be dependent on wave height (as well as wind).[21] As the sea surface wind speed is known by using the XMOD algorithm, this improves the accuracy of predicting the range of wave heights of the ocean area where the TS-X data is acquired by following an empirical formula of type $\lambda_{\text{cut}} = (R/V)\sqrt{aH_s + bU^2}$, where λ_{cut} is the cut-off wavelength, R and V is the satellite altitude and velocity respectively, H_s is significant wave height and U the wind speed, as given in Ref. 21.

If the predicted significant wave height (predicted by the azimuth cut-off wavelength) is below 3.5 m, Eq. (1) is used and if above 4.5 m, Eq. (2) is used, and to provide a certain degree of safety, a buffer zone of the correlated azimuth cut-off predicted significant wave heights between 3.5 and 4.5 m is used [Eq. (3)], where a simple combination of Eqs. (1) and (2) is used. The XWAVE function can then be defined as follows:

For significant wave heights predicted to be below 3.5 m,

$$H_s1 = a_1 \cdot \sqrt{E \cdot \tan\theta} + v \cdot a_2 \cdot U_{10} + a_3. \tag{1}$$

For significant wave heights predicted to be above 4.5 m,

$$H_s2 = a_4 \cdot \sqrt{E \cdot \tan\theta} + v \cdot a_5 \cdot U_{10} + a_6 \cdot \cos(\alpha) + a_7. \tag{2}$$

For significant wave heights predicted to be between 3.5 and 4.5 m,

$$H_s3 = \frac{H_s1 + H_s2}{2}. \tag{3}$$

The parameter $E = \int_{k_{\min}}^{k_{\max}} \int_0^{2\pi} \overline{P}(k,\theta) \mathrm{d}k\mathrm{d}\theta$ is the integrated energy of the derived wave number spectrum with corresponding wavelength limits $k_{\min} = (2/L_{\min})$; $L_{\min} = 30$ m, and $k_{\max} = (2/L_{\max})$; $L_{\max} = 600$ m, obtained by Fourier analysis on the TS-X data. The box size of the analysis varies; for coastal applications, the box size is 1024 pixel using a spatial averaged Strimap image by a factor of 2, which gives a box length of about 2.6 km.

The parameter θ is the incidence angle v, is a unitary coefficient with unit (s), and U_{10} is the sea surface wind speed at 10 m height obtained by the XMOD algorithm.[16] And α, as described earlier, is the peak wave direction related to the satellite flight path (azimuth direction) ($0 \text{ deg} \leq \alpha \leq 90 \text{ deg}$). The cosine function correction depending on α is only applied for values above 40 deg. The coefficients a_0 to a_6 are tuning parameters, which are found after fitting the TS-X derived parameters E, α, and θ with significant wave height given by the *in situ* buoy wave measurements using the least squares method.

4 Coastal Wave Fields Extraction

In coastal areas sea-state properties usually change rapidly in the spatial domain due to the underlying bathymetry. Increased complexity of the sea floor leads to even higher spatial variability of sea-state properties.

Measurement of the highly variable sea-state properties of coastal areas can be difficult; buoys can only estimate the sea properties of the exact location where they are located.

Wave fields derived by coastal numerical wave models seem at first glance to be a suitable choice for coastal ocean area analysis and validation of results, when calculated using as input ideal conditions—a proper fine up-to-date fine meshed bathymetry—and as boundary initial proper wave and wind conditions. For quality estimation, aside the performance of the model itself, up-to-date fine resolution bathymetry is needed together with initial boundary conditions: sea-state parameters or spectra, wind fields, wave current field, etc. And of course, all the input information needs to be accurate. For the wave and wind conditions at the boundary normally taken from global scale wave models, some inaccurate results can occur, especially in storm situations where models have more difficulty in predicting accurately the correct significant wave height or the time at which the storm occurs.

For the case of the bathymetry input, for some areas, the bathymetry available can be outdated and not representative of the real bathymetry, or in some locations the bathymetry is rapidly changing in time and becomes outdated and unsuitable very fast because the ground floor is sand or mud and therefore is easily affected by transport and erosion. For this reason modeling is not a straightforward task.

In our study we choose a complex coastal area in the North Sea as our test site for coastal wave field extraction from TS-X data using the XWAVE algorithm and test how it would perform in coastal waters. The location chosen was the North Sea near the Elbe estuary on the coast of Germany.

The North Sea area is a shallow water depth ocean area, with a few hundred meters depth maximum, in comparison to the open ocean as for example the Atlantic, Pacific, or Indian, where water depth is of a few kilometers. In Fig. 1 we can observe the underlying bathymetry of the North Sea area near the coast of Germany and its complexity in the coastal areas.

TS-X SAR imagery over the ocean is acquired regularly, especially near and over the coast of Germany, e.g., over Helgoland island, Elbe estuary, Sylt, and Cuxhaven. At some locations in the

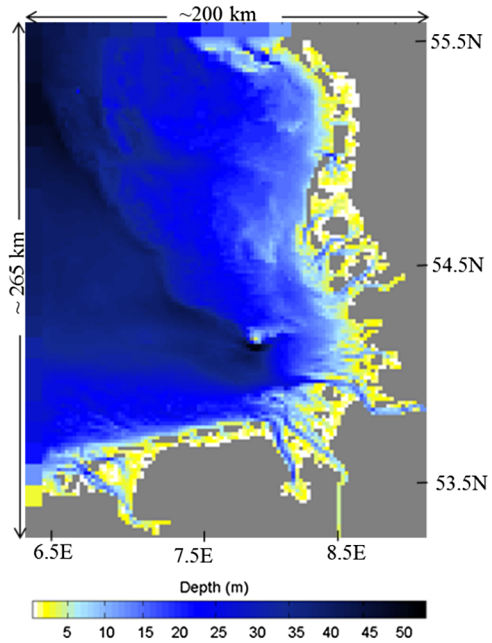

Fig. 1 Bathymetry with a resolution of 1 nautical mile for the North Sea area near the coast of Germany.

Fig. 2 ©Google Earth overview of the North Sea area near Germany and the position of the wave measuring buoys shown by the North West European Shelf Operational Oceanographic System.

North Sea, buoy wave measurement devices are available. Figure 2 shows an overview of the North Sea area near the coast of Germany and the wave measuring buoys located in that area. The buoy near the Elbe estuary (referred as Buoy Elbe) is used in our paper for comparison of results.

We present two cases studies (Secs. 4.1 and 4.2) where the derived significant wave height and peak wavelength wave field are compared to *in situ* wave measurements and one case study (Sec. 4.3) where the derived wave height is compared to numerical wave model results.

The first two case studies are taken at different times in nearly the same location west from the Elbe estuary and are compared to *in situ* buoy measurements and numerical wave model results provided by the DWD. The first case presents a high sea-state situation and the second one a moderate sea-state situation. The third case is located in the Elbe estuary during moderate sea-state conditions. higher-resolution coastal model (*k*-model).

The third case was chosen to be verified by wave model results because it is the most complex coastal area of all the test cases. The variation of the sea-state conditions will be strongly present in this area in any wave conditions.

4.1 *Case Study 1: High Sea State*

The first case study is the analysis of TS-X Stripmap VV polarized image acquired under high sea-state conditions between the Helgoland island and the Elbe estuary on December 9, 2011, at 5:42 UTC (see Fig. 3). The TS-X acquisition is collocated with a buoy (Buoy Elbe) (54.02°N, 8.11°E) visible in the middle of the image (see Fig. 2). The measured buoy significant wave height is of 5.7 m at 6:02 UTC and the derived significant wave height from the TS-X data for the same location gives a slight overestimation, 6.0 m. The derived wave peak period from the TS-X data using the deep water relationship is 11.6 s against 11.1 s given by the buoy.

The comparison of the sea-state parameters given by the buoy and the ones derived from the TS-X subscene acquired over the position of the buoy are shown in Table 1. Additionally, the sea-state parameters for the nearest grid point to the buoy location (54°N, 8.2°E) of the DWD wave model results are given. The significant wave height given by the wave model for that location is 4.1 m.

The underwater topography of the area imaged by TS-X is shown in Fig. 4 (red box). The water depth varies between values of ~40 and <5 m in the bottom part of the TS-X acquisition. It is expected high variation on ocean wave heights due to the complex under water topography,

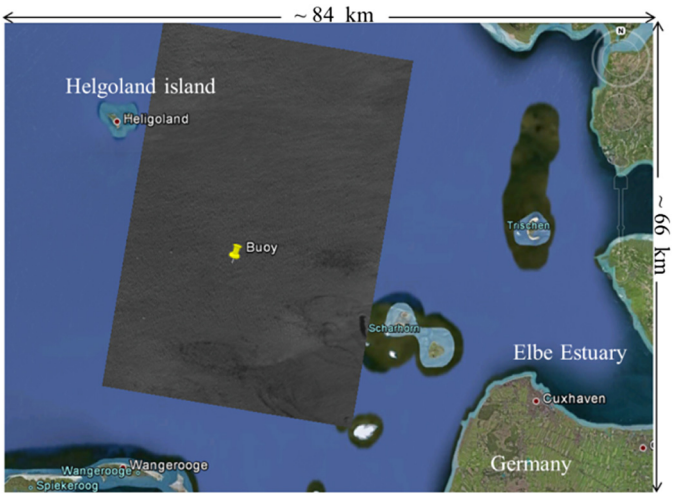

Fig. 3 TS-X Stripmap VV pol. image acquired on December 9, 2011, at 5:42 UTC near the island of Helgoland located in the North Sea, near the coast of Germany shown on Google Earth©.

Table 1 Summary of the sea-state parameters derived from the TS-X data acquired over the buoy location (Fig. 3) (TS-X Stripmap VV pol. image acquired on December 9, 2011. at 5:42 UTC), compared to *in situ* buoy wave measurements and the results from the wave model running at DWD for the nearest grid point from buoy location at coordinates 54.0N 8.2E.

	Hs (m)	*Tp* (s)	Λp (m)	*Dir* (°)	U_{10} (m/s)
DWD	4.1	13.5	285	307	18.5
Buoy	5.7	11.1	195	—	—
TS-X	6.0	11.6	210	298	21.1

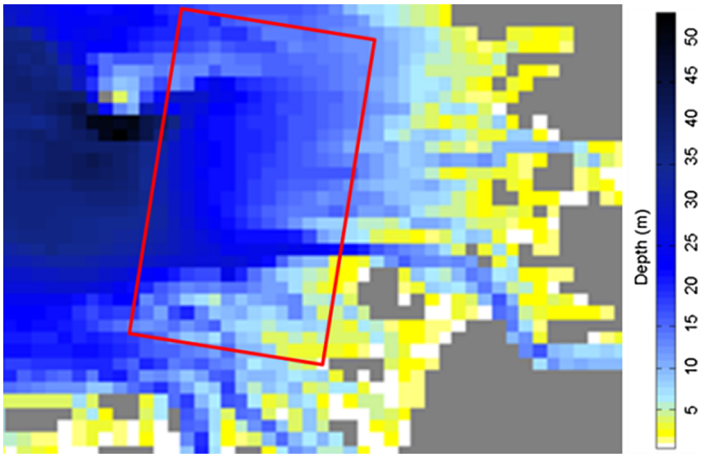

Fig. 4 Underlying bathymetry for the same area shown in Figure 4. The red box corresponds to the area of the TS-X acquisition.

varying from higher values of wave heights in deeper locations to lower values in shallow water locations. The exception will be in the ocean area shadowed by the Helgoland island (Fig. 5).

To give us further insight for the meteo-marine conditions during the TS-X acquisition we use the wave model results provided by the DWD. The wave height field (0.75 deg × 0.75 deg spatial resolution) results by the wave model at DWD for the North Sea area are given (see

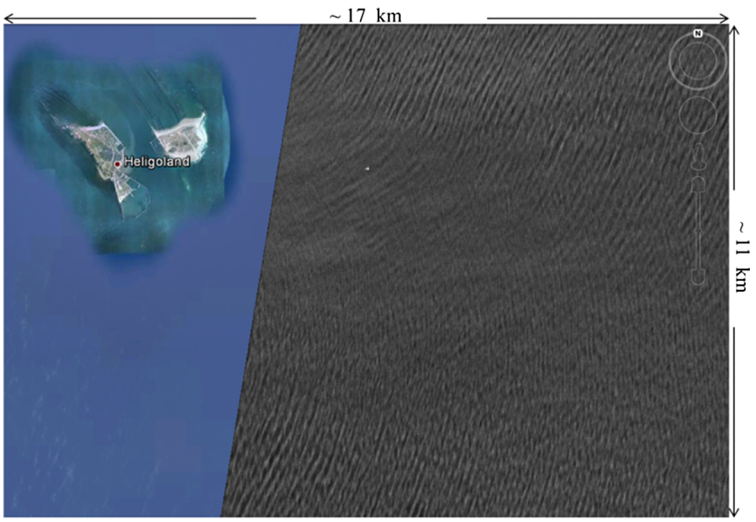

Fig. 5 Zoom into the TS-X Stripmap VV pol. image acquired on December 9, 2011, at 5:42 UTC near Helgoland island in the north coast of Germany shown on Google Earth©.

Figs. 6 and 7). The neighboring grid points to the nearest DWD grid buoy location in the west (54.0°N, 7.5°E), the north (54.8°N, 8.2°E), and the northwest (54.8°N, 7.5°E) indicate significant wave heights of 5.4, 2.2, and 6.3 m, respectively.

We can also determine from the DWD wave model data that the east propagating wave field is mainly wind-sea driven. For the nearest grid point of the buoy/TS-X acquisition, the wave model wind-sea height component is 4.0 m against 0.9 m for the swell component (see Figs. 6 and 7). In Fig. 8, the TS-X derived wind field is shown. The values of wind speed are very high, varying between 20 and 25 m/s.

This case shows that although wind speed is an important contribution in the algorithm, the derived integrated energy related to the modulation of the sea surface is more important, and although wind speed is constantly high over the analyzed area, the derived significant wave height has a variation from lower values of 2 to 6 m as it is shown in Fig. 9.

In this case study we can further observe the shadow effect provoked by the Helgoland island shown in Fig. 5. In Fig. 9 is visible the drop of derived significant wave height and peak wavelength values for the location where the shadow effect is present.

In the area acquired by the TS-X, which is about 32 km by 46 km, the derived significant wave height varies between 6.8 down to 2.2 m.

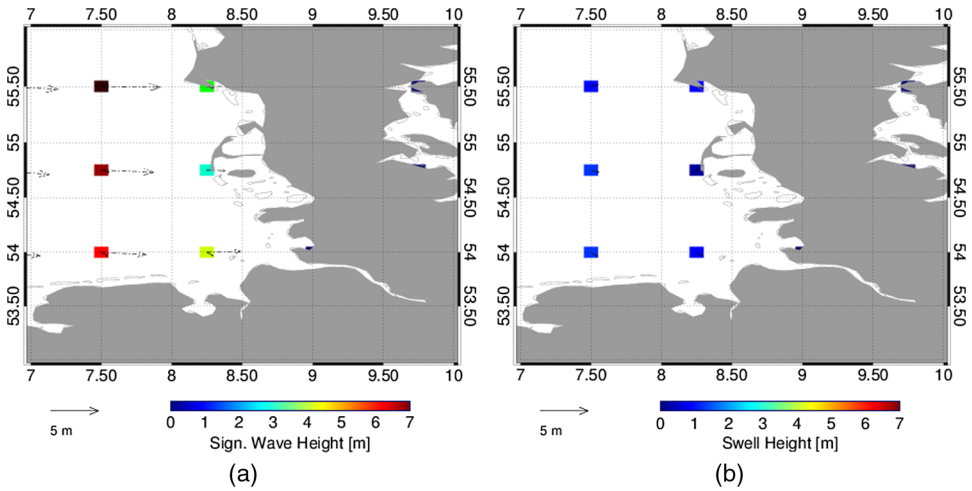

Fig. 6 Significant wave height field (a) swell wave height (b) given by the DWD wave model on December 9, 2011, at 6:00 UTC.

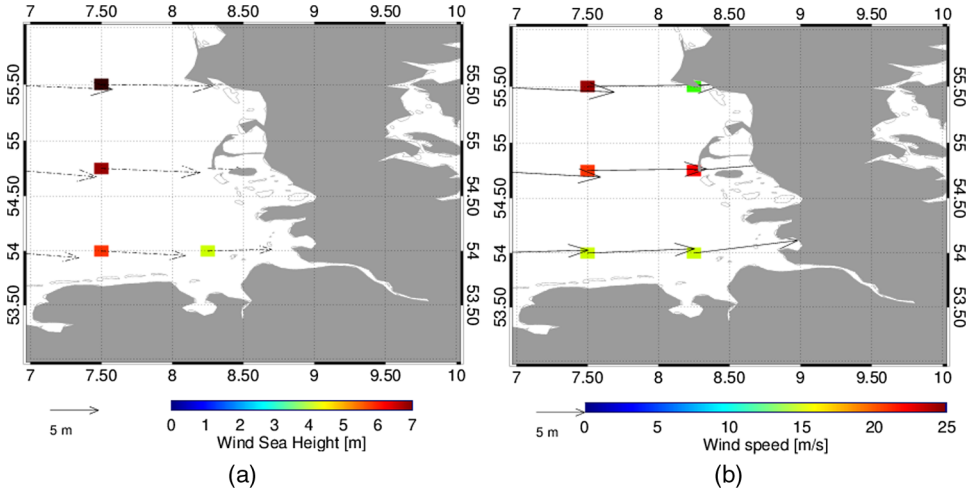

Fig. 7 Wind sea height (a) and wind field (b) given by the DWD wave model on December 9, 2011, at 6:00 UTC.

For this case of high sea state and high sea surface variability, we additionally analyzed four small subscenes (2.6 km × 2.6 km) taken at different locations of the TS-X acquisition (see Fig. 9). The analyses of the four subscenes are shown in Fig. 10.

Case (a) is located in an open sea area in the upper part of the TS-X acquisition and has a derived significant wave height of 5.1 m and a wave peak wavelength of 165 m. Only one wave system is detected in the 2-D derived spectrum from the subscene.

Subscene (b) is located in the area where the wave fields reunite after being diffracted round the Helgoland island. The case is a cross-sea situation where the two wave systems with different directions can be visualized in the derived 2-D spectrum. The significant wave height for this case is 3.6 m and the wave peak wavelength is 139 m.

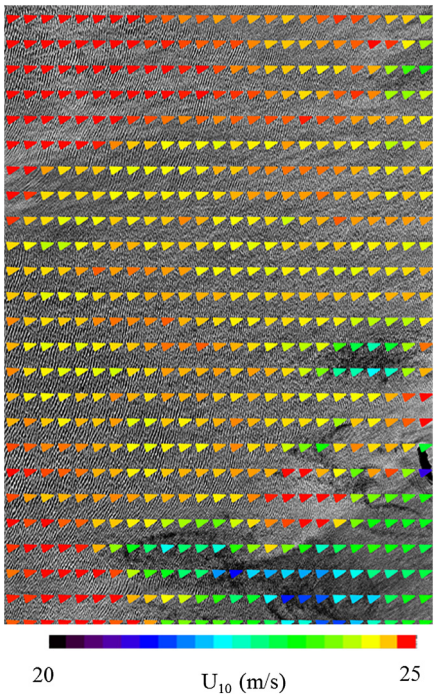

Fig. 8 Wind field derived using the XMOD algorithm for the TS-X Stripmap VV pol. acquired on December 9, 2011, at 5:42 UTC.

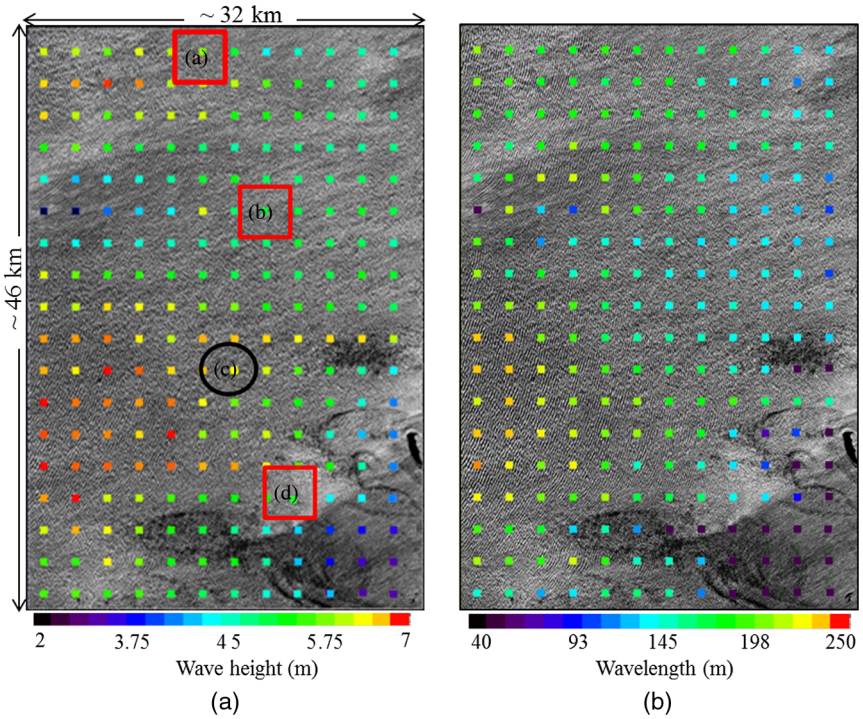

Fig. 9 Significant wave height field (a) and wave peak wavelength field (b) derived from TS-X Stripmap image VV pol. acquired on December 9, 2011, at 5:42 UTC using a 2.6 km × 2.6 km box. The red boxes and black circle (location of the buoy) are the cases presented in Fig. 10.

Subscene (c) is located at the position of the buoy. Only one wave system is detected in the 2-D spectrum derived from the subscene. The significant wave height for this case is 6.0 m, as referred to previously. Table 1 gives additional information for this case.

Case (d) is located near shallower waters in the bottom part of the TS-X acquisition near the coast, where sea surface signatures can be seen in the SAR image caused by the underlying bathymetry. The derived significant wave height for this case is 4.4 m. The wave peak wavelength for this case is the lowest of all the cases with 134 m. Two wave systems are detected in the 2-D spectrum with similar wave direction but different wavelengths, as we can observe in the subscene, some ocean waves located in the bottom have shorter wavelengths.

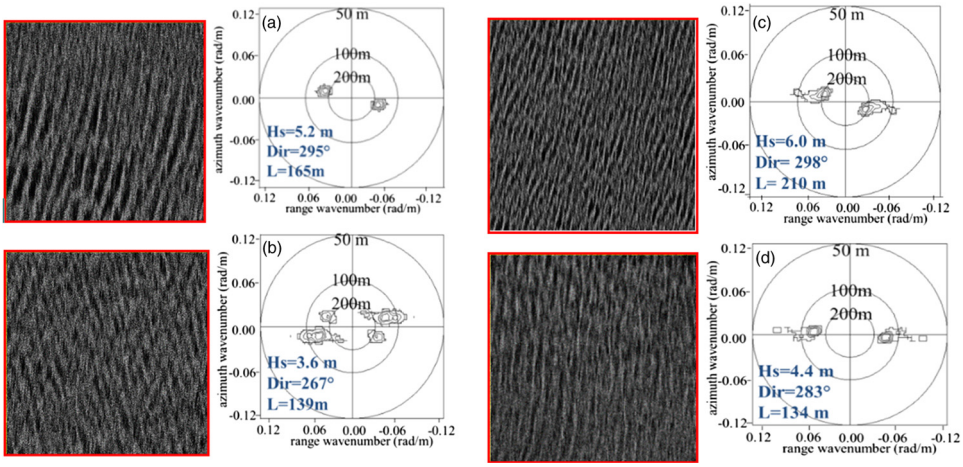

Fig. 10 TS-X (2.6 × 2.6) km subscenes from the TS-X VV pol. image acquired on December 9, 2011, at 5:42 UTC (see Fig. 6).

4.2 *Case Study 2: Moderate Sea State*

The second case presented in this paper is the analysis of the TS-X Stripmap VV polarized image acquired during moderate sea-state conditions on February 22, 2012, at 17:01 UTC nearly in the same location of the first case study. The buoy is located in the west edge of the TS-X data image (see Fig. 11). The underlying bathymetry is shown in Fig. 12.

The wave model data provided by the DWD for the North Sea area for the closest time of the TS-X acquisition are shown in Figs. 13 and 14. The data show that the wave field propagating near the TS-X acquisition for the nearest grid point has a significant wave height of 2.3 m and is mainly wind-sea driven. With a wind-sea wave height of 2.0 m, the wind speed used in the wave model is 14 m/s for the nearest grid point. Wave propagation is to the northeast, which suggests that the wave field is generated by local winds as the mainland is in the south.

The subscene analyzed at the buoy location and the derived 2-D spectrum from the subscene can be seen in Fig. 15. The sea-state parameters derived from the TS-X data, the buoy location, and the ones given by the buoy are given in Table 2.

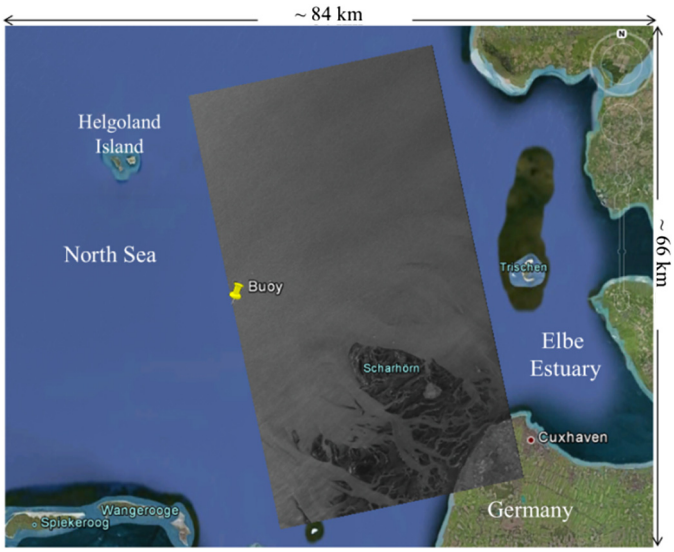

Fig. 11 TS-X Stripmap VV pol. acquired on February 22, 2012, at 17:01 UTC over a buoy west from the Elbe estuary shown on Google Earth©.

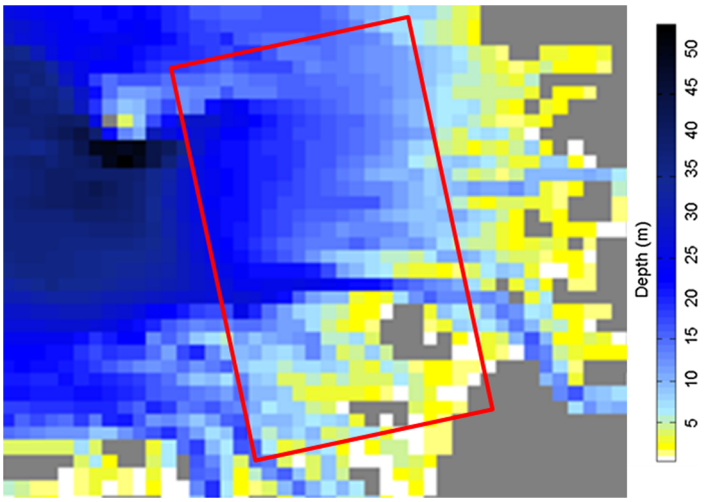

Fig. 12 Underlying bathymetry for the same area in Fig. 11. The red box corresponds to the area of the TS-X acquisition.

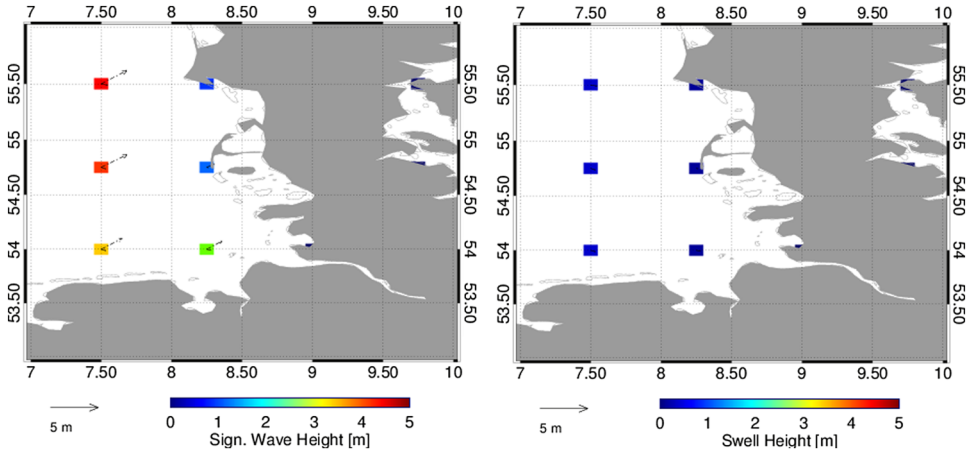

Fig. 13 Significant wave height field (a) and swell wave height (b) given by the DWD wave model on February 22, 2012, at 18:00 UTC.

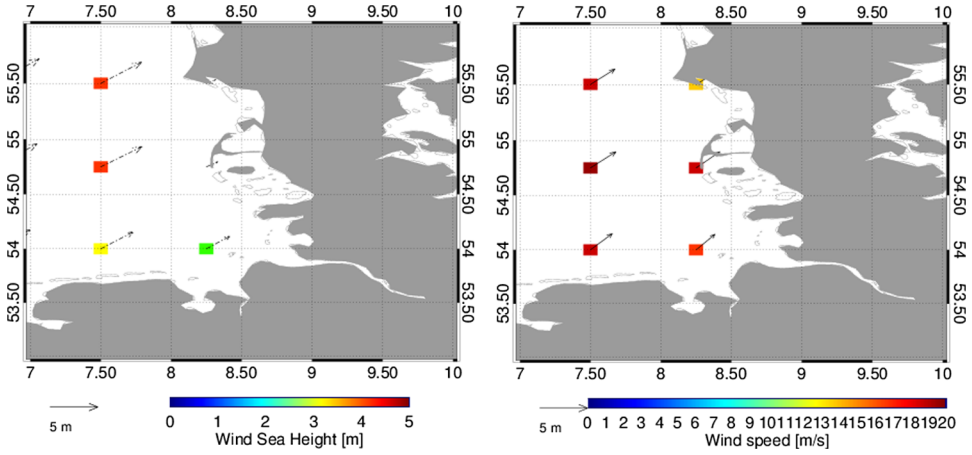

Fig. 14 Wind sea height (a) and wind field (b) given by the DWD wave model on February 22, 2012, at 18:00 UTC.

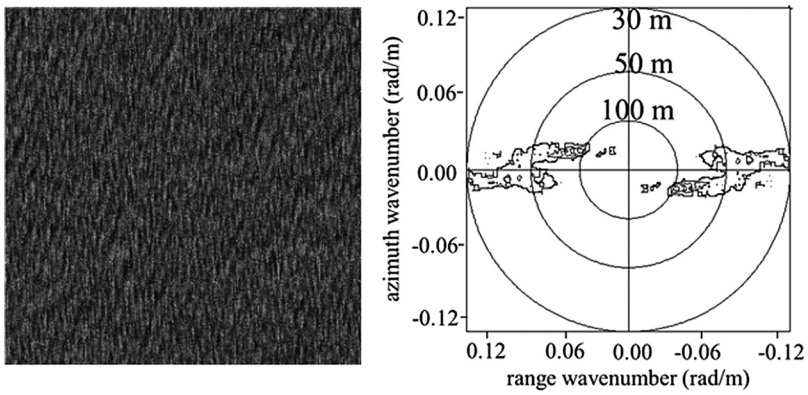

Fig. 15 TS-X subscene taken from the TS-X Stripmap VV pol. acquired on February 22, 2012, at 17:01 UTC over the Elbe buoy (a) and the derived SAR 2-D spectrum (b).

Table 2 Summary of the sea-state parameters derived from the TS-X data acquired over the buoy location (Fig. 11) (TS-X Stripmap VV pol. acquired on February 22, 2012, at 17:01 UTC) compared to *in situ* buoy wave measurements and results from the wave model running at DWD for the nearest grid point from buoy location at coordinates 54.0N 8.2E.

	Hs (m)	*Tp* (s)	Λp (m)	Dir (°)	U_{10} (m/s)
DWD	2.3	9.2	132	286	14.7
Buoy	1.9	8.3	108	—	—
TS-X	1.9	7.8	95	280	16.7

The derived significant wave height at the buoy location is 1.9 m, which is the same value of wave height given by the buoy. The derived wave peak period from the TS-X data is 7.8 s and the wave peak period measured by the buoy is slightly higher, 8.3 s.

In Fig. 16, the derived wind fields using the XMOD algorithm on TS-X data are shown.

In Fig. 17(a), the derived significant wave height field and the corresponding wave peak wavelength field from the TS-X data are shown. The values of derived significant wave height vary from values of 2.2 m in the area north from the buoy, down to values of height of 0.3 m in the shallower areas.

Values of 2.2 m are more in agreement with the DWD wave model results. For this case under moderate sea-state conditions, it was possible to measure a variability of almost 2 m.

In Fig. 17(b), the corresponding wave peak wavelength is shown. It follows in general the same variability tendency of the significant wave height wave field with shorter wavelengths derived where wave height is lower.

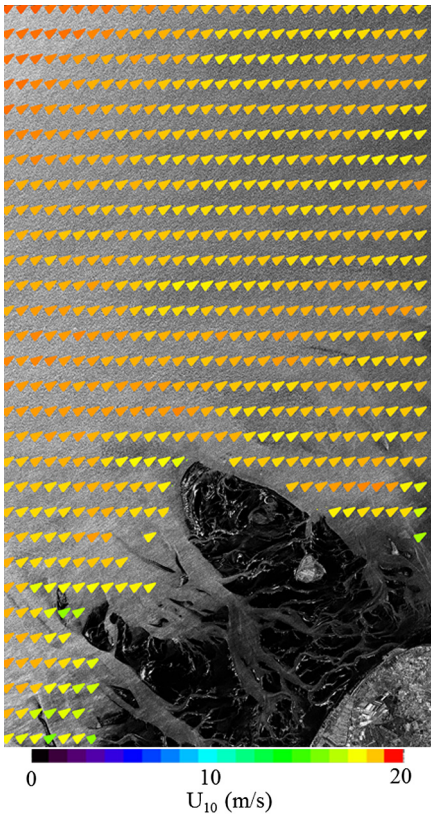

Fig. 16 Wind field derived using the XMOD algorithm for the TS-Stripmap VV pol. acquired on February 22, 2012, at 17:01 UTC over a buoy west from the Elbe estuary.

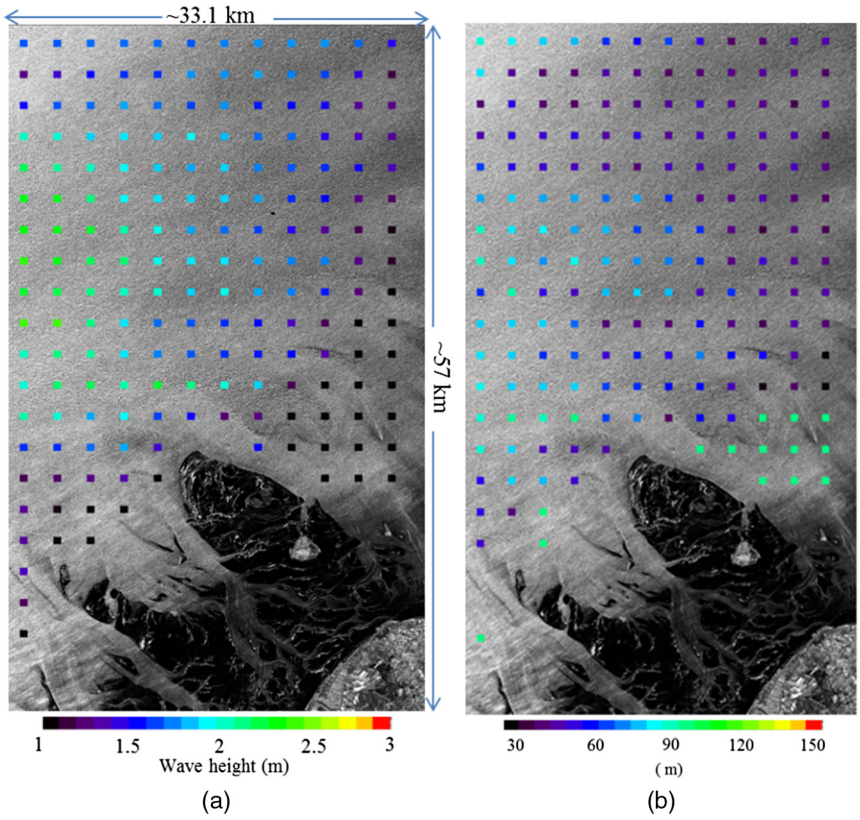

Fig. 17 Significant wave height wave field derived from the TS-X Stripmap VV pol. image acquired over the buoy near the Elbe estuary acquired on February 22, 2012, at 17:01 UTC using a 2.6 km × 2.6 km box (a) and wave peak wavelength field (b).

4.3 *Case Study 3: Coastal Wave Model Comparison*

The third case study is the analysis of the TS-X Stripmap HH polarization acquired over the Elbe estuary North Germany, on November 21, 2008, at 17:01 UTC (Fig. 18).

The underlying bathymetry for the same area is shown in Fig. 19. The water depth for the area acquired by the TS-X varies from 0 to ~15 m. The Elbe estuary, as stated previously, is a very complex coastal area; it has a high number of sand banks that are constantly changing due to tides and currents, which leads to the fact that the bathymetry in this area is rapidly changing over time.

The low values of water depth in the area of the TS-X acquisition greatly enhance the importance of the complexity of the underlying bathymetry. Any change in the bathymetry will have a strong effect on the ocean waves.

The TS-X data in this case are acquired under moderate sea-state conditions with a significant wave height provided by the wave model from DWD of 2.4 m for the nearest grid point of the TS-X acquisition (54N 8.25E).

The wave model results are shown in Figs. 20 and 21. The wave model data show that this case is also mainly wind-sea driven. The wind-sea component is 2.2 m against 0.9 m for the swell wave component.

The wind speed values given by the DWD model for the North Sea area vary between 13 m/s (in the nearest grid point location to the TS-X acquisition) and 17 m/s in the northwest grid point (Fig. 21).

Applying the XMOD algorithm to the TS-X data, it is possible to observe the variability of sea surface wind speed (Fig. 22). The highest values of wind speed are of about 14 m/s in the brighter area (left side of the image) and about 5 m/s in the darkest area of the image (right side of the image). The wind field extraction and the variability observed are

Fig. 18 TS-X HH pol. Stripmap image acquired on November 21, 2008, at 17:01 UTC over the Elbe estuary shown on Google Earth ©.

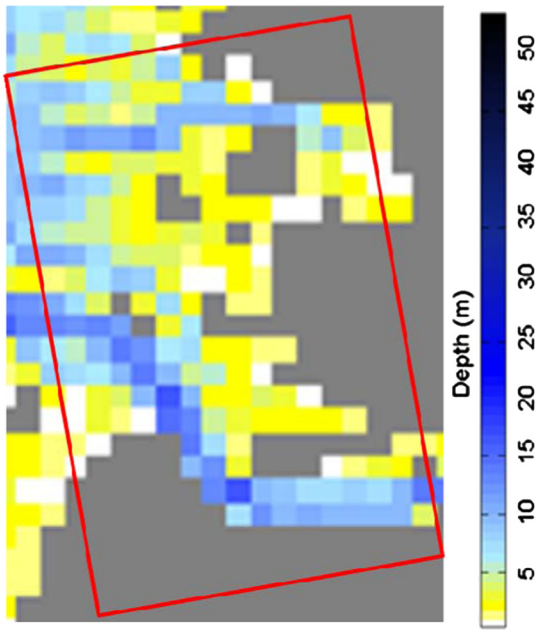

Fig. 19 Underlying bathymetry for the same area shown in Fig. 18. The red box corresponds to the TS-X acquisition.

important as we recall the derived sea surface wind speed by the XMOD is used as input in the XWAVE algorithm.

The significant wave height field derived from the TS-X data is for this case study obtained by shifting the analysis box by 1.3 km. The TS-X wave analysis box resolution is a 1024 pixel box with a spatial averaged subscene by a factor of 2, which corresponds to an area of ~2.5 km.

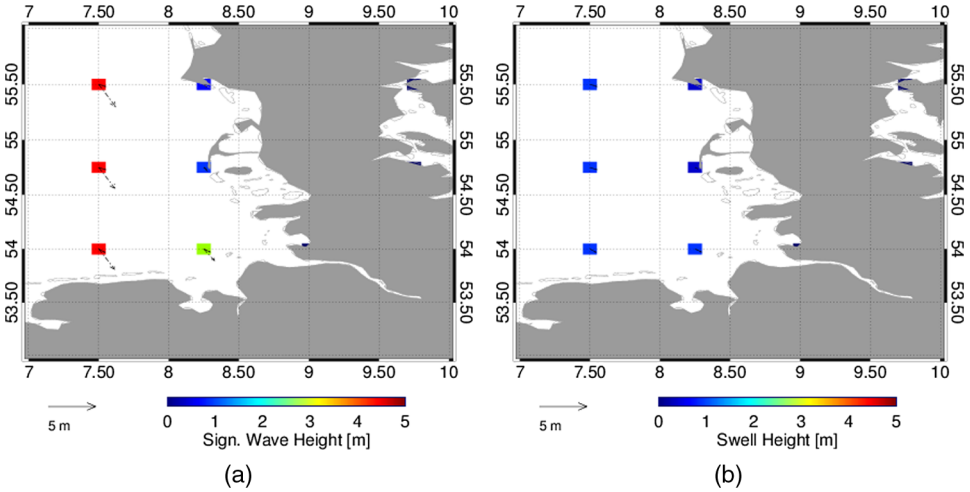

Fig. 20 Significant wave height field (a) and the swell wave height field (b) given by the DWD wave model on November 21, 2008, at 17:01 UTC.

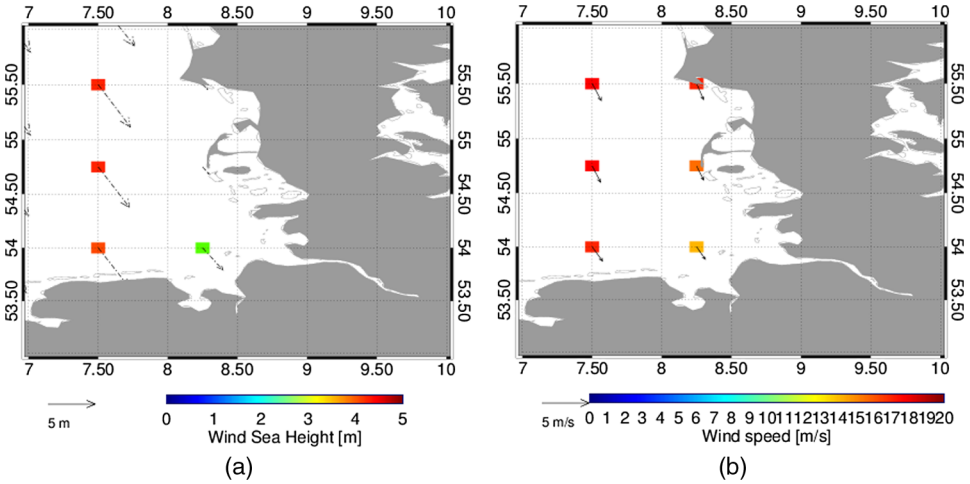

Fig. 21 Wind sea height field (a) and the wind speed field (b) given by the DWD wave model on November 21, 2008, at 17:01 UTC.

The wave model (k-model), as it was previously described in Sec. 2, is set to run with 1 nautical mile resolution (~1.9 km).

The comparison with a numerical coastal model with fine resolution and up-to-date bathymetry is valued to assess the stability of the significant wave height estimation over all the wave field. The sea state and wind input information for the boundary conditions for the K-model are given by the DWD wave model data.

Significant wave height in the derived TS-X wave field [Fig. 23(a)] and the significant wave height results from the numerical model (Fig. 24) follow the same trend of significant wave height values though the analyzed area, with derived significant wave height values of 2.2 m against 2.0 m given by the wave model and down to derived values of 0.5 m against values of 0.3 m given by model for the same locations. The corresponding wave peak wavelength field of the derived significant wave height wave field is given in Fig. 23(b).

We can observe the change in wave peak wavelength from longer waves in deeper locations to shorter wavelengths in shallower locations. Again in this case, although the wind variation in the area analyzed is high, there is a balance between the derived spectral parameter E and the

Fig. 22 Wind field derived using the XMOD algorithm for the TS-X acquisition taken on November 21, 2008, at 17:01 UTC over the Elbe estuary.

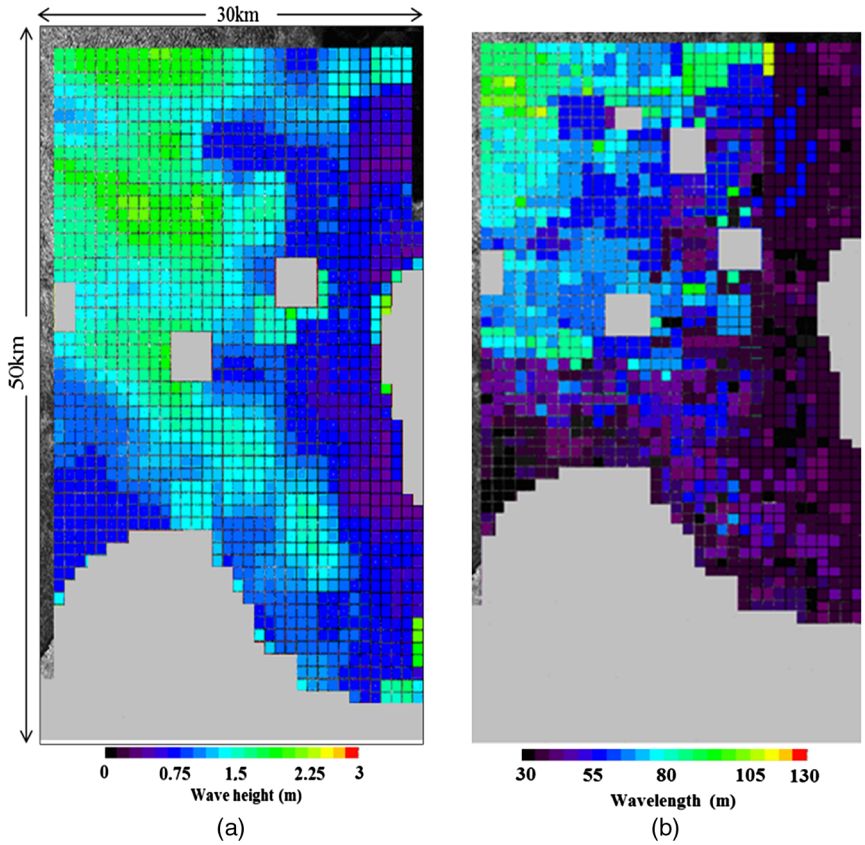

Fig. 23 Significant wave height wave field derived from the TSX HH pol. Stripmap image acquired on November 21, 2008, at 17:01 UTC (a) and the corresponding derived peak wavelength field (b).

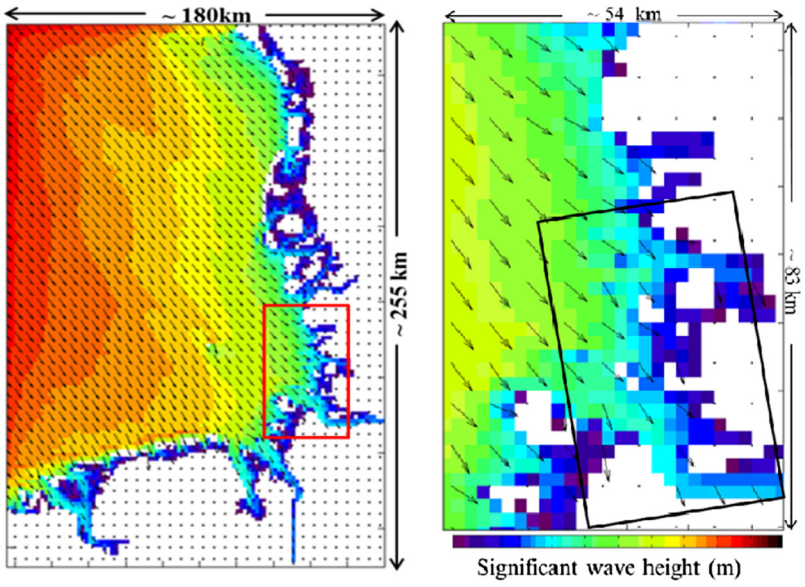

Fig. 24 Numerical wave model results for the North Sea area, near the coast of Germany, with a resolution of 1 nautical mile. The red box corresponds to the area of the zoom shown on the right. (a) Zoom into the left image, the black box corresponds to the area of the TS-X acquisition. (b) Plots courtesy of Dr. Andrey Pleskachevsky.

derived wind speed, in the XWAVE algorithm which provides a stable derived significant wave height as it is confirmed by the numerical wave models results.

5 Conclusions

TS-X Stripmap imagery acquired in coastal areas is analyzed using the XWAVE algorithm; significant wave height fields with high resolution including the spatial information on wave variations were derived. The respective wave peak wavelength field is derived additionally by Fourier analysis of the TS-X data.

In general, the results look promising. Three case studies were analyzed under different sea-state conditions. In the first case study, the TS-X image is acquired under high sea state. The case shows high sea-state variability in the spatial domain, with derived significant wave height changing from 2.0 up to 6.0 m within a distance of <30 km. The significant wave height derived at the location of the buoy is 6 against 5.7 m given by buoy.

In the second case, under moderate sea state, the significant wave heights derived from TS-X data and the one given by the buoy are the same with the value of 1.9 m.

In the third case study, the derived wave field is compared to numerical wave model results.

Significant wave height fields derived from TS-X data and calculated by the coastal model follow the same variation tendency of values over the field, with higher values of significant wave height in deeper locations and lower values of significant wave height in shallower waters.

In conclusion, significant wave height derived from coastal TS-X imagery using the XWAVE algorithm shows good agreement with *in situ* buoy wave measurements and numerical wave model results. The results derived for the case studies analyzed provide values of significant wave height within the range level of the performance which was achieved during the validation and tuning procedure using deep water buoys, but further testing in a larger scale is needed. Nevertheless it is shown here that wave fields derived from TS-X SAR imagery using the XWAVE algorithm can be a useful tool in the analysis of coastal ocean areas and that the derived information from the data is suitable to characterize the spatial domain in highly variable sea-state conditions.

6 Outlook

Further testing using data acquired in coastal areas and different types of wave climates need to be performed to assert the performance of the algorithm in more wave conditions. Coastal wave fields derived from TS-X SAR imagery will continually be compared for different wave and wind conditions with fine meshed numerical wave model results and with *in situ* buoy wave measurements. A more detailed study needs to be done on the information extracted as to how the wind-sea and swell and the wind contribution influences the algorithm in high variable wave conditions found in coastal areas.

Acknowledgments

Buoy data are provided by the North West European Self Operational Oceanography System http://www.noos.cc/. The numerical wave model data were provided by Dr. Thomas Bruns from the German Weather Center (DWD), and TS-X data are acquired under the science proposal OCE1070.

References

1. W. Alpers, D. Ross, and C. Ruffenach, "On the detectability of ocean surface waves by real and synthetic aperture radar," *J. Geophys. Res.* **86**(C7), 6481–6498 (1981), http://dx.doi.org/10.1029/JC086iC07p06481.
2. K. Hasselmann and S. Hasselmann, "On the nonlinear mapping of an ocean wave spectrum into a synthetic aperture radar image spectrum," *J. Geophys. Res.* **96**(C6) 10713–10729 (1991), http://dx.doi.org/10.1029/91JC00302.
3. H. Krogstad, "A simple derivation of Hasselmann's nonlinear ocean synthetic aperture radar transform," *J. Geophys. Res.* **97**(C2), 873–885 (1992), http://dx.doi.org/10.1029/91JC03010.
4. G. Engen and H. Johnson, "SAR-ocean wave inversion using image cross spectra," *IEEE Trans. Geosci. Rem. Sens.* **33**(4), 1047–1056 (1995), http://dx.doi.org/10.1109/36.406690.
5. S. Hasselmann et al., "An improved algorithm for the retrieval of ocean wave spectra from SAR image spectra," *J. Geophys. Res.* **101**(C7), 16615–16629 (1996), http://dx.doi.org/10.1029/96JC00798.
6. C. Mastenbroek and C. F. de Valk, "A semi-parametric algorithm to retrieve ocean wave spectra from synthetic aperture radar," *Geophys. Res.* **105**(C2), 3497–3516 (2000), http://dx.doi.org/10.1029/1999JC900282.
7. J. Schulz-Stellenfleth, S. Lehner, and D. Hoja, "A parametric scheme for the retrieval of two-dimensional ocean wave spectra from synthetic aperture radar look cross spectra," *J. Geophys. Res.* **110**(C5), C05 004.1–C05 004.17 (2005), http://dx.doi.org/10.1029/2004JC002822.
8. J. Schulz-Stellenfleth, T. König, and S. Lehner, "An empirical approach for the retrieval of integral ocean wave parameters from synthetic aperture radar data," *J. Geophys. Res.* **112**(C3), 1–14 (2007), http://dx.doi.org/10.1029/2006JC003970.
9. X. Li, S. Lehner, and T. Bruns, "Ocean wave integral parameter measurements using Envisat ASAR wave mode data," *IEEE Trans. Geosci. Rem. Sens.* **49**(1), 155–174 (2011), http://dx.doi.org/10.1109/TGRS.2010.2052364.
10. S. Brusch, P. Held, and S. Lehner, "Monitoring river estuaries and coastal areas using TerraSAR-X," presented at *Proc. of the OCEANS 2009-EUROPE*, Bremen, Germany (2009).
11. S. Brusch et al., "Underwater bottom-topography in coastal areas from TerraSAR-X data," *Int. J. Rem. Sens.* **32**(16), 4527–4543 (2011), http://dx.doi.org/10.1080/01431161.2010.489063.
12. G. Diaz Mendez et al., "Wind and wave observations off the south Pacific Coast of Mexico using TerraSAR-X imagery," *Int. J. Rem. Sens.* **31**(17), 4933–4955 (2010), http://dx.doi.org/10.1080/01431161.2010.485217.

13. X. Li, S. Lehner, and W. Rosenthal, "Investigation of ocean surface wave refraction using TerraSAR-X data," *IEEE Trans. Geosci. Rem. Sens.* **48**(2)830–840 (2010), http://dx.doi.org/10.1109/TGRS.2009.2033177.
14. M. Bruck and S. Lehner, "Sea state measurements using TerraSAR-X data," in *2012 IEEE International Geoscience and Remote Sensing Symposium (IGARSS)*, Munich, Germany, pp. 7609–7612 (2012).
15. S. Lehner, A. Pleskachevsky, and M. Bruck, "High resolution satellite measurements of coastal wind field and sea state," *Int. J. Rem. Sens.* **33**(23), 7337–7360 (2012), http://dx.doi.org/10.1080/01431161.2012.685975.
16. Y. Ren et al., "An algorithm for the retrieval of sea surface wind fields using X-band TerraSAR-X data," *Int. J. Rem. Sens.* **33**(23), 7310–7336 (2012), http://dx.doi.org/10.1080/01431161.2012.685977.
17. M. Schwerdt et al., "TerraSAR-X calibration results," in *Proc. of the IEEE Geoscience and Remote Sensing Symp.*, Boston, Vol. 2, pp. 205–208 (2008).
18. H. Breit et al., "TerraSAR-X SAR processing and products," *IEEE Trans. Geosci. Rem. Sens.* **48**(2), 727–740 (2010), http://dx.doi.org/10.1109/TGRS.2009.2035497.
19. "WAMDIG: the WAM model—A third generation ocean wave prediction model," *J. Phys. Oceanogr.* **18**(12), 1775–1810 (1988), http://dx.doi.org/10.1175/1520-0485(1988)018<1775:TWMTGO>2.0.CO;2.
20. C. Schneggenburger, H. Günther, and W. Rosenthal, "Spectral wave modeling with nonlinear dissipation: validation and applications in a coastal tidal environment," *Coast. Eng.* **41**(1–3), 201–235 (2000), http://dx.doi.org/10.1016/S0378-3839(00)00033-8.
21. P. W. Vachon, H. E. Krogstad, and J. S. Paterson, "Airborne and spaceborne synthetic aperture radar observations of ocean waves," *Atmos.-Ocean.* **32**(1)83–112 (1994), http://dx.doi.org/10.1080/07055900.1994.9649491.

Miguel Bruck received his diploma degree in geophysics-oceanography/meteorology from the Faculty of Sciences at the Lisbon University, Lisbon, Portugal, in 2006. Received his master's in oceanographic remote sensing from the same university in 2008. He worked at the Wave Energy Group at the Laboratory for Energy and Geology (LNEG), Lisbon, Portugal, from 2006 to 2008. He joined the German Aerospace Center (DLR), Wessling, Germany, in 2009, working toward the PhD degree with the Remote Sensing Technology Institute at the SAR Oceanography Group. His current research interests include the development of algorithms to derive sea state information from SAR images.

Susanne Lehner received the MSc degree in applied mathematics from Brunel University, Uxbridge, United Kingdom, in 1979 and the PhD degree in geophysics from the University of Hamburg, Hamburg, Germany, in 1984. She was a research scientist with the Max-Planck Institute for Climatology, Hamburg, and joined the German Aerospace Center (DLR/DFD), Wessling, Germany, in 1996. She is currently a research scientist in marine remote sensing with the Remote Sensing Technology Institute (DLR/IMF), German Aerospace Center, working on the development of algorithms determining marine parameters from synthetic aperture radars